Proceedings of the ASME 2018 Power Conference
POWER2018
June 24-28, 2018, Lake Buena Vista, FL, USA

POWER2018-7558

CFD ANALYSIS OF STALL IN A WELLS TURBINE

Kellis Kincaid
Applied Computational Engineering Laboratory
Department of Mechanical Engineering
University of Alabama
Tuscaloosa, Alabama 35487

David W. MacPhee *
Applied Computational Engineering Laboratory
Department of Mechanical Engineering
University of Alabama
Tuscaloosa, Alabama 35487
Email: dwmacphee@ua.edu

ABSTRACT

The Wells turbine is a self-rectifying device that employs a symmetrical blade profile, and is often used in conjunction with an oscillating water column to extract energy from ocean waves. The effects of solidity, angle of attack, blade shape and many other parameters have been widely studied both numerically and experimentally. To date, several 3-D numerical simulations have been performed using commercial software, mostly with steady flow conditions and employing various two-equation turbulence models. In this paper, the open source code OpenFOAM is used to numerically study the performance characteristics of a Wells turbine using a two-equation turbulence model, namely the Menter SST model, in conjunction with a transient fluid solver.

NOMENCLATURE

Co Courant number
N Number of blades
R_{tip} Radius of blade tip
S Mean rate of strain
T Net torque on turbine
T* Torque coefficient
U* Flow coefficient
U_{tip} Tangetial velocity of rotor tip
V Inlet velocity
c Chord length
f Rotational force term
g Tip gap
h Hub-to-tip ratio
p Thermodynamic pressure
s Turbine solidity
t Time
u Velocity vector
x Position vector
y+ Dimensionless wall distance
μ Dynamic viscosity
$\tilde{\nu}$ Spallart-Allmaras modified eddy viscosity
ρ Density
τ Reynolds stress tensor
Ω Angular velocity

INTRODUCTION

The demand for electrical power has increased at a staggering pace over the last century, and only recently have the negative effects of conventional conversion methods come to be studied and understood. These effects, such as pollution and other environmental damage, have naturally led to an increase of interest in clean, renewable energy. Three such renewable sources, hydroelectric, wind and solar energy, have been employed to great effect and continue to make increases in efficiency while lowering cost. Another promising source is found in our oceans. With the majority of Earth's surface covered by water, there is an immense amount of untapped energy in the tides, currents, and

*Address all correspondence to this author.

waves of the seas. Waves are particularly appealing, as they are readily available both near the shore and in the open ocean.

There are two plausible techniques for wave energy conversion: the first utilizes a fixed bobber to drive a hydraulic pump [1], while the second uses an Oscillating Water Column (OWC) device to power a turbine. An OWC typically consists of a large concrete structure, either built into the shore or on top of the seabed, which forms a chamber above sea level that is open to the water below. At the top of the chamber, a small outlet is formed and a turbine is placed inside. As a wave passes the OWC, the rise in water outside of the chamber causes the level inside to rise as well. The air inside is compressed, and its forced through the turbine to generate power. The opposite occurs when a wave trough passes the column; the level inside the chamber drops, the air is rarefied, and more is pulled in to equalize the pressure. Due to the cyclic nature of airflow in an OWC, the turbine involved needs to either have self-rectifying properties, or a valving system must be used to divert air through only one side of the turbine. The first method stands out for being simpler and more cost-effective, and has been thoroughly studied since the invention of the Wells turbine by A.A. Wells in the 1970's. The Wells turbine uses a symmetric blade profile to achieve the self-rectifying characteristics necessary for operation in an OWC device. Typically, four to eight short blades are mounted on a large rotor, providing a simple and durable construction.

The combination of an OWC device and Wells turbine offers many advantages. As there are no moving parts in the water, OWCs create no obvious threat to wildlife, and may in fact be beneficial, providing cover for fishes and potentially acting as a man-made reef. Arrays of OWC's can be incorporated into breakwater structures, used to shield shorelines and harbors from waves. They can also be located further from shore, either built on or anchored to the sea floor. Finding a suitable area is not much of a challenge, as the OWC structure can be optimized to accommodate the typical conditions of almost any location with reliable wave activity. The chamber of the device can be sized to resonate at the typical wave frequency in a region, which can increase power output if executed correctly [2]. The simplicity afforded by the design could offer low construction and maintenance costs. Since the turbine and associated machinery operate in air, not water, the service life of the equipment is extended greatly. However, there are several drawbacks, including noise pollution and construction difficulty. The turbines produce a loud noise in operation [3], which can be resolved by locating the devices further from shore, or in a remote location. Construction difficulties typically arise during bad weather, when temporary platforms are often inadequate and waves can be dangerous for workers. This can be addressed by assembling major components off location, and transporting them to the site where they can be erected more quickly.

Several examples of energy conversion using this turbine exist. An installation in Mutriku, Spain incorporated 16 units into a breaker wall for a choppy harbor. Opened in 2011, the station is capable of producing 300kW and required few modifications to the structure it was built into [4]. In 1999, near Islay, Scotland, the Queen's University of Belfast built a 75kW prototype to investigate the viability of wave energy conversion in the area. The project was a success, and in 2011 Queen's University and privately owned Wavegen collaborated to build a 500kW plant in the same location. The plant features two Wells turbines encased in an OWC device, built into the cliff face and extending about six meters below sea level. To prevent construction difficulties, the majority of the plant was excavated and constructed behind a layer of rock, which shielded the site from bad weather. The rock was later removed as the project neared completion, allowing the finishing touches to be added [5].

Previous experimental and computational studies of the Wells turbine have demonstrated a capability for modest efficiency, especially under the low flow rates and frequencies which are typically produced by OWCs. Steady-state numerical simulations, such as those of Torresi et. al. [6] and Kim et. al. [7] have shown the effects of turbine parameters such as tip gap and blade profile on performance. These cases typically use a commercial code such as FLUENT, and typically employ a k-ε turbulence model. Experimental studies by Setoguchi et. al. [3] tested several variations of a Wells turbine against another turbine type, showing better characteristics at lower flow coefficients. Transient numerical simulations have been completed by Setoguchi et. al. [8] to investigate various flow phenomena detected in experimental setups. Variations such as passive guide vanes have been experimentally shown by Darabi and Poriavali to increase the efficiency and torque further [9].

This study builds upon the others mentioned herein by making use of transient simulations to better assess the stall behavior of Wells turbines at higher flow conditions. Through utilization of an open-source CFD software and post-processing relevant fields such as pressure and turbulent eddy viscosity, the mechanicsm of turbine blade stall can be better analyzed than if utilizing only steady-state simulation techniques.

1 Modeling and Discretization

As air is the working fluid, the governing equations for fluid flow consist of the Reynolds-Averaged Navier Stokes Equations, written as follows:

$$\nabla \cdot \mathbf{u} = 0 \tag{1}$$

$$\rho \left[\frac{\partial \mathbf{u}}{\partial t} + \mathbf{u} \cdot \nabla \mathbf{u} \right] = -\nabla p + \nabla \cdot (2\mu \mathbf{S} + \tau) + \rho \mathbf{f} \tag{2}$$

Here, the former is mass conservation and the latter momentum conservation. Implicit in these equations is the assumption

of incompressible Newtonian flow. The fluid time-averaged pressure and velocity are denoted by p and $\mathbf{u}$, respectively, while $\mathbf{S}$ denotes the mean rate of strain tensor and τ the Reynolds stress tensor.

In this study, the Menter shear stress transport (SST) model is used to approximate turbulence [10]. The Menter SST model consists of two transport equations involving k and ω, which correlate to the turbulent eddy viscosity ν_t through the Boussinesq assumption. This method was compared to others such as Spallart-Allmaras and $k-\varepsilon$, and selected for its higher accuracy with respect to previous experimental results.

The body force term in Eqn. 2 is modified in the present study so that simulations can be performed in a rotating reference frame. Assuming constant angular velocity, this term contains both the centrifugal and Coriolis forces and is written as follows:

$$\mathbf{f} = -2\Omega \times \mathbf{u} - \Omega \times (\Omega \times \mathbf{x}) \tag{3}$$

where Ω is the angular velocity and $\mathbf{x}$ is the position vector. The numerical solutions presented herein were executed using the open source code Foam Extend (a branch of OpenFOAM [11]), version 3.2. A three dimensional domain was created using the blockMesh utility, and solved in a single rotating reference frame moving with the turbine at a constant angular velocity of $\Omega = (0, 0, 209.44)$ rad/s, equivalent to 2000rpm.

All simulations in this study were conducted using the PISO algorithm [12], with a second-order cell centered finite-volume method for spatial discretization and an implicit Euler time discretization. Time step size was specified to be 1E-06 seconds, which resulted in a maximum Courant number of 1.1 through the full range of inlet speeds. However, the average Courant number was much lower than this, typically on the order of 1E-03.

The turbine simulated in this study has been studied experimentally in [13], and has the following characteristics:

Number of blades, N = 8
Constant chord length, c = 0.125m
Tip radius, R_{tip} = 0.3m
Tip-to-hub ratio, h = $\frac{2}{3}$
Solidity, s = 0.6366
NACA 0015 blade profile
Tip gap, g = 1% of chord length.

Due to the radial symmetry of the turbine, the system could be effectively modeled by considering only one blade and incorporating cyclic or periodic boundary conditions on side walls. To ensure independence from inlet and outlet boundaries, the domain was extended for seven chord lengths upstream, and nine chord lengths downstream of the airfoil, similar to that in [6]. Additionally, further entry and exit lengths were added with slip boundary conditions to further isolate the case from inlet and outlet effects. The inlet velocity was set using a constant absolute velocity, mapped to a relative velocity coincident with the rotating reference frame. The rotor and stator surface velocities were set to zero in the rotating and stationary reference frames, respectively. All outlet variables were constrained to have a zero gradient normal to the outlet surface.

The recorded quantity for all simulations is the rotor torque, T. In order to compare the results to existing data in [13], the torque coefficient, T^*, is then defined as follows:

$$T^* = 8\frac{T}{\rho\Omega^2 R_{tip}^5} \tag{4}$$

Here, a factor of 8 is included as the computational domain includes only one blade. The properties of the working fluid are assumed to be those of air at sea level, with a temperature of 15°C.

While constructing the mesh, effort was taken to ensure grid independence. Calibration simulations were conducted at a wide range of cell counts, from 5×10^3 to upwards of 10^6. For mesh independence tests, the inlet velocity is set to conform to a flow coefficient of $U^* = 0.20$, where the flow coefficient is defined as:

$$U^* = \frac{V}{U_{tip}} \tag{5}$$

Here, U_{tip} is the tip rotor velocity. Using this inlet velocity, several simulations were conducted modifying cell count and progression ratios near surfaces to achieve achieve favorable y^+ values for accurate turbulence field calulations. From these tests, a domain was chosen with a grid size of 386,960 cells, selected as a good balance of accuracy, stability and computation time. The resulting mesh as shown on the surface of the blade can be seen in Fig. 1. Due to the clustering of cells near relevant surfaces, the average y-Plus varied from 10 on the blade to 83 on the rotor hub, all within the acceptable range of values.

For each simulation, instantaneous torque values were recorded every 5 time steps, and averaged after quasi-steady results reached. These torque values were obtained during run-time by integrating surface (both pressure and viscous) forces over the rotor (blade and hub). Figure 2 shows a typical variation in torque coefficient as simulation progresses transiently, with U^* = 0.200.

2 Results and Discussion

In order to test the current simulation scheme, the simulations in [6] were replicated, that is, with nine different flow coefficients ranging from 0.100 to 0.300, spanning the performance

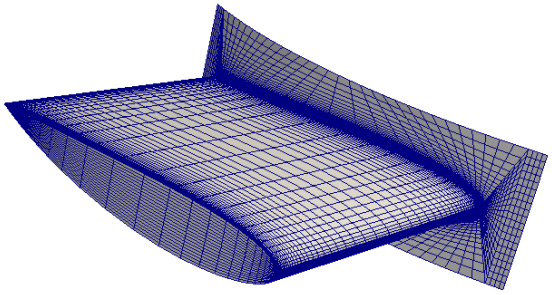

FIGURE 1: Cell spacing near the blade and hub surface.

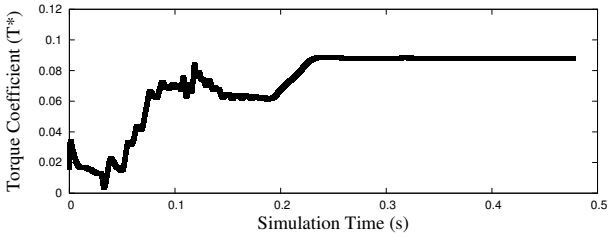

FIGURE 2: Typical variation in T^* as the simulation progresses.

curve determined in previous literature. The results from this study are seen in Fig. 3, which also shows the experimental values from [13] and previous simulations from [6].

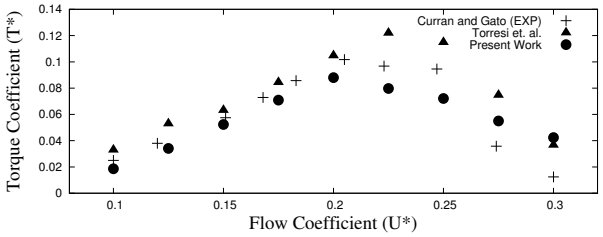

FIGURE 3: Results from our simulations, as compared to previous simulations [6] and experiments [13].

The carefully constructed mesh and simulation parameters allow an excellent agreement with experimental data across most of the useful flow range of the turbine. From U* = 0.100 to 0.250, the average error relative to the corresponding experimental value is 14.7%. At higher flow values, the current model begins to significantly overpredict performance. The present results are at least as accurate as those from the more computationally

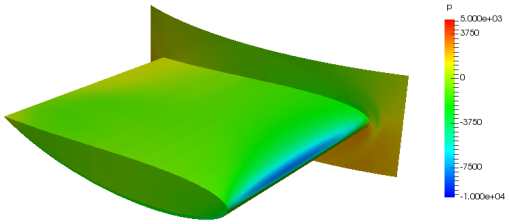

FIGURE 4: Pressure contour on turbine blade surface.

intensive studies taken by Curran et. al. at most points. Some of this may be attributable to the slightly more rigorous treatment of turbulence using the two-equation turbulence model described above.

To more deeply analyze the results of the study, and the stall phenomenon, post-processing of the simulations was conducted for all cases using the native paraFoam viewer (a paraview wrapper for OpenFOAM). In all images, the scaling of each individual variable is consistent throughout the study unless otherwise noted. Additionally, OpenFOAM utilities were used to collect force and moment data from the turbine.

First, we look at the pressure variation on the blades themselves, as the thermodynamic pressure p is the main driver of torque. Note that pressure in the following figures is actually p/ρ, as it is common with incompressible solvers to divide through by density. Figure 4 shows the pressure distribution on the blade surface and rotor hub for the case where $U^* = 0.200$.

For cases with lower inlet velocities, typically below U* = 0.225, the pressure distribution varies little after the flow stabilizes around the blade. However as velocity was increased past stall, it was noticed that the moment produced by the turbine began to vary periodically. Figure 5 shows the torque coefficient of three separate cases as simulation time progresses.

These oscillations appear to be approximately sinusoidal, with a period near one hundredth of a second. To determine the underlying cause of this phenomena, the pressure field was examined at four points spaced approximately one quarter period apart in one cycle. A magnified plot of the torque coefficient for U* = 0.250 is shown in Fig. 6, along with the four points selected for further investigation.

Upon examination of the pressure field at these four points, a bubble of pressure was observed detaching from the downstream blade face once per period. A series of images showing this process are given in Fig. 7.

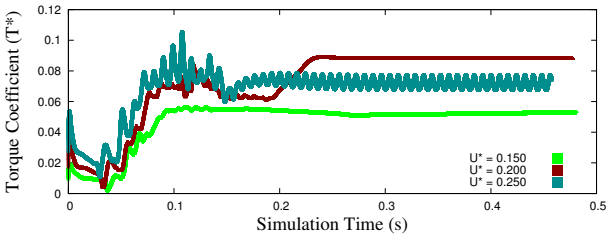

FIGURE 5: Comparison of torque coefficients pre- and post-stall.

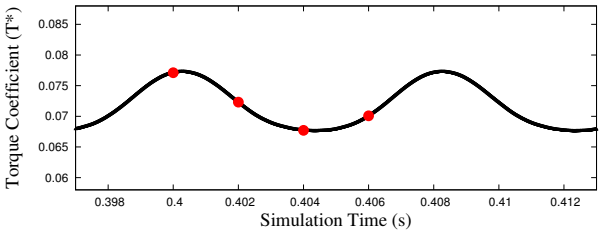

FIGURE 6: Magnified torque curve for U* = 0.250.

To determine the cause of these shedding events, a velocity contour was plotted in a plane parallel with the blade chord at a distance of 0.26m from the center of rotation. The resulting field is shown in Fig. 8 for 0.404 seconds of simulation time, which corresponds to the local minima in the torque coefficient oscillation.

There is a region of reversed flow on the downstream face of the blade, as shown in Fig. 8. This backflow region expands and contracts out of phase with the pressure oscillations shown in Fig. 7. This is likely the source of the vortex shedding, as the reversal region pushes incoming flow up and away from the blade face. In turn this causes a less favorable pressure differential across the blade, contributing to the decrease in torque observed for high flow coefficients.

These fields are quite different from those of lower flow coefficients, where a steady state is often achieved within half a second of the simulation start. The stabilized field of the U* = 0.200 case is shown in Fig. 9, at 0.400 seconds of simulation time. Additionally, a velocity contour is presented in Fig. 10 for 0.404 seconds of simulation time.

Neither the vortex shedding or the flow reversal are present in this case. This leads to a much higher performance than in the previously examined case, caused partially by the high suction pressure on the upstream leading face of the blade.

From the above analysis it is obvious that a Wells turbine experiences stall in much the same way as an airfoil in external flow. Past a certain angle of attack, or flow coefficient (the equivalent for the present work), flow reversal will occur on the blade surface, leading to vortex shedding, increased drag and reduced

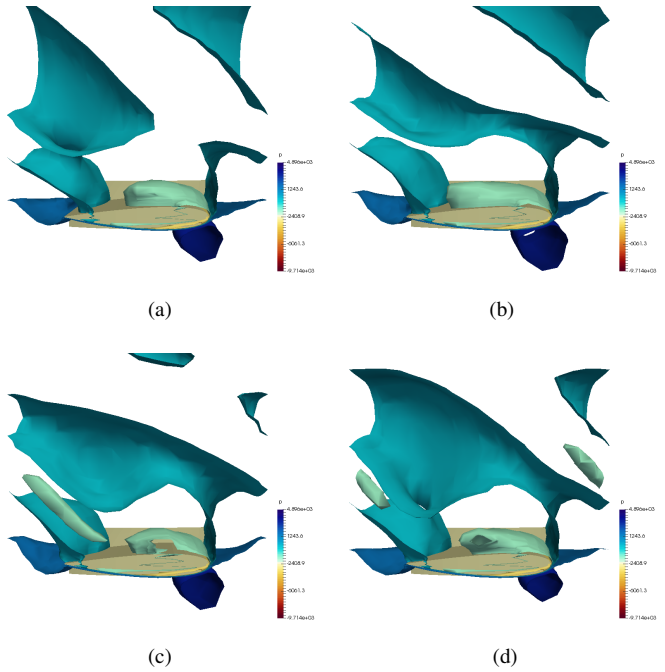

FIGURE 7: Progression of pressure bubble during oscillations, U* = 0.250.

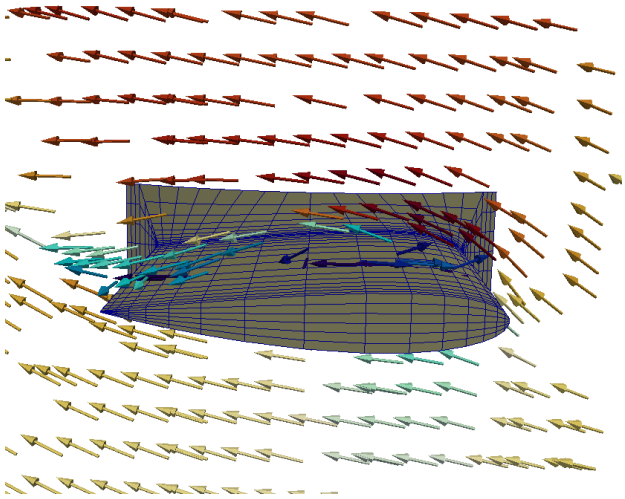

FIGURE 8: Velocity contour for U* = 0.250 at 0.404s.

performance.

The turbulence kinetic energy, k, is solved in the process of evaluating the Menter SST equations. In addition to the pressure and velocity fields, it is often useful to examine the k field to glean further details about flow behavior. In Fig. 11, the k field is shown viewed from the end of the blade.

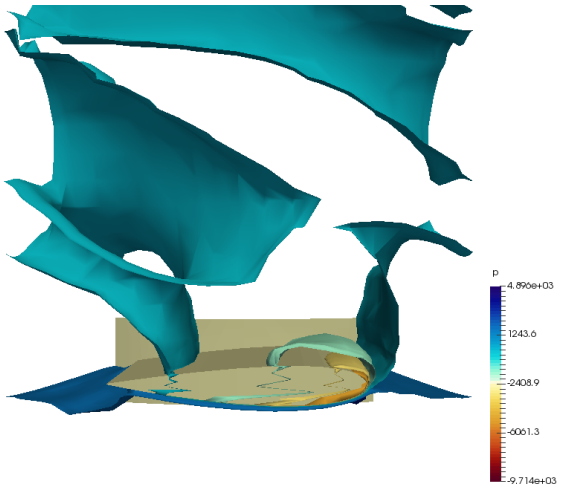

FIGURE 9: Steady pressure field for U* = 0.200.

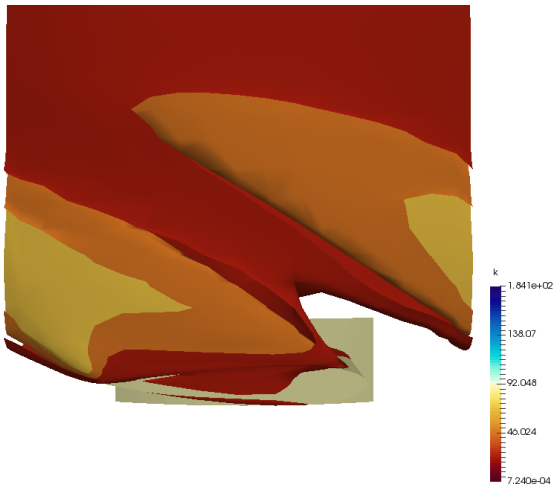

FIGURE 11: Turbulence kinetic enegy field for U* = 0.200.

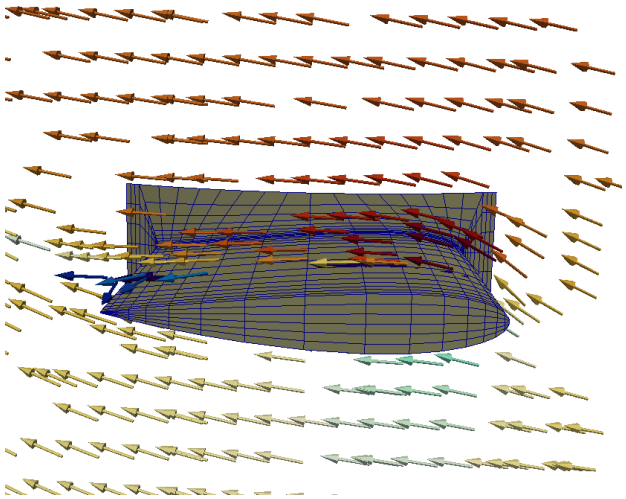

FIGURE 10: Steady velocity field for U* = 0.200.

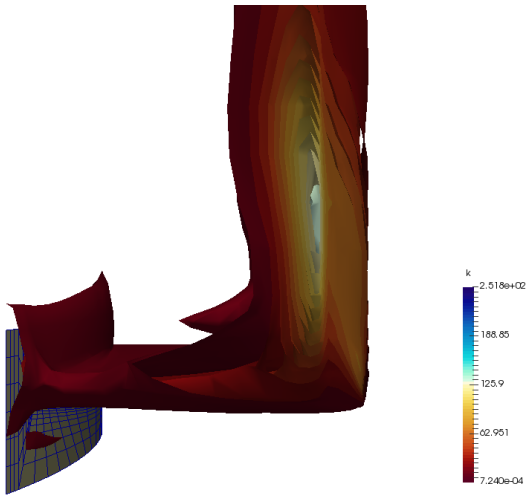

FIGURE 12: Rear view of k field for U* = 0.200.

From this we see a streak of high turbulence near the downstream face of the blade, which is expected. However, when viewed from the rear as in Figs. 12 and 13, it is more evident why the high flows suffer reduced performance. The U* = 0.200 case exhibits very low k values on the inner half of the blade, compared to the U* = 0.250 case where the high k streak extends nearly from the rotor hub to the blade tip. This extended area of high turbulent losses likely inhibits favorable flow conditions from developing, greatly inhibiting turbine performance.

These results indicate that not only is it possible to simulate a Wells turbine using reasonable cell counts, but realistic results can be realized by carefully constructing grids to conform to wall models. In this study, the Menter SST model was used to simulate the Wells Turbine across a range of flow conditions with excellent results, by using transient flow, a PISO algorithm paired with a two-equation turbulence model, and a reasonable (386,960) volume count in the computational domain.

3 Conclusions

In this study, a second-order finite volume solver was used to simulate a well-documented geometry of a Wells turbine using a relatively small mesh size for rapid computing. A two-equation turbulence model was employed to further decrease computational complexity, and a transient solver was used to capture any unsteady phenomena in the flow. The results obtained agree well

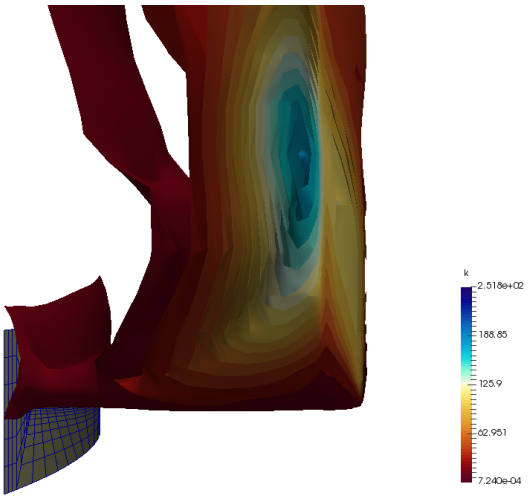

FIGURE 13: Rear view of k field for U* = 0.250.

with a previously conducted experimental study in the area of peak torque production, and are in some regions more accurate than other studies which assume steady-state analysis and require an order of magnitude more cell volumes. This can be attributed to the suitability of certain mesh characteristics to the modeling schemes used herein. Additionally, the possible causes of stall were identified, which is the first step towards mitigating the issue and increasing performance. The validation of the performance of the code in this case will allow future transient simulations to be completed to pursue novel design improvements of the turbine.

REFERENCES

[1] Lin, Y., Bao, J., Liu, H., Li, W., Tu, L., and Zhang, D., 2015. "Review of hydraulic transmission technoligies for wave power generation". *Renewable and Sustainable Energy Reviews,* ***50***, pp. 194–203.

[2] Curran, R., 2008. "Ocean wave energy systems design: Conceptual design methodology for the operational matching of the wells air turbine". 15th ISPE International Conference on Concurrent Engineering.

[3] Setoguchi, T., Takao, M., and Kaneko, K., 2000. "A comparison of performances of turbines for wave power conversion". *International Journal of Rotating Machinery,* ***6***, pp. 129–134.

[4] Journal, M., 2011. "First commercial wave power plant opens".

[5] Heath, T., 1999. "Stuck on the limpet". Water Power Magazine.

[6] Torresi, M., Camporeale, S., Strippoli, P., and Pascazio, G., 2008. "Accurate numerical simulation of a high solidity wells turbine". *Renewable Energy,* ***33***, pp. 735–747.

[7] Kim, T., Kaneko, T. S. K., and Raghunathan, S., 2000. "Numerical investigation on the effect of blade sweep on the performance of wells turbine". *Renewable Energy,* ***25***, pp. 235–248.

[8] Setoguchi, T., Kinoue, Y., Kim, T., Kaneko, K., and Inoue, M., 2003. "Hysteretic characteristics of wells turbine for wave power conversion". *Renewable Energy,* ***28***, pp. 2113–2127.

[9] Darabi, A., and Poriavali, P., 2007. "Guide vanes effect of wells turbine on o.w.c. wave power plant operation". Vol. 1, World Congress on Engineering.

[10] Menter, F. R., 1994. "Two-equation eddy-viscosity turbulence models for engineering applications". *AIAA journal,* ***32***(8), pp. 1598–1605.

[11] Jasak, H., Jemcov, A., and Tukovic, Z., 2007. "Openfoam: A c++ library for complex physics simulations". In International Workshop on Coupled Methods in Numerical Dynamics, pp. 1–20.

[12] Issa, R., 1986. "Solution of the implicitly discretised fluid flow equations by operator splitting". *Journal of Computational Physics,* ***62***, pp. 40–65.

[13] Curran, R., and Gato, L., 1997. "The energy conversion performance of several types of wells turbine designs". Vol. 211, Institution of Mechanical Engineers Journal of Power and Energy, pp. 133–145.

ACKNOWLEDGMENT

The authors acknowledges support from the National Science Foundation's Research Experience for Undergraduates (REU) program in conducting this research.